2005

Temperature dependence of the magnetism in Fe/Cu(001)

Axel Enders
University of Nebraska-Lincoln, a.enders@me.com

D. Repetto
Max Planck Institut für Festkörperforschung

D. Peterka
Max Planck Institut für Festkörperforschung

Klaus Kern
Max Planck Institut für Festkörperforschung, k.kern@fkf.mpg.de

Temperature dependence of the magnetism in Fe/Cu(001)

A. Enders,* D. Repetto, D. Peterka, and K. Kern
Max Planck Institut für Festkörperforschung, Heisenbergstr. 1, D-70569 Stuttgart, Germany
(Received 9 May 2005; published 31 August 2005)

The correlation between morphology and magnetism of ultrathin epitaxial films is investigated by a combined study of variable temperature scanning tunneling microscopy, magneto-optical Kerr effect measurements, and Kerr microscopy under ultrahigh vacuum condition. The magnetization reversal of the films was studied as a function of temperature by imaging the propagation of Bloch domain walls *in situ*. It is demonstrated on the example of fcc Fe films grown at 120 K on Cu(001) that changes in the morphology of the films during annealing are directly reflected in modified magnetic properties. Competing pinning mechanisms for the domain wall propagation are identified. The energy barrier distribution controlling the propagation of domain walls at low temperature is determined.

DOI: 10.1103/PhysRevB.72.054446 PACS number(s): 75.30.Gw, 75.50.Bb, 75.60.Ej, 75.60.Jk

I. INTRODUCTION

One of the main goals of the research on thin film magnetism is to find correlations between the structure and the magnetic properties of ultrathin epitaxial films. A detailed understanding of such a relationship is not only of basic interest but would allow us to tailor magnetic properties of more complex structures for application in devices. The majority of experiments performed so far show that the observed phenomena are often unique to a particular combination of film and substrate, and principles of general relevance are rare.[1,2] Moreover, in some cases the published results are partly contradictory, indicating that subtle deviations in the preparation condition, substrate quality, etc. can cause significant changes in the film morphology or magnetism.

The magnetization reversal process by domain wall propagation in ultrathin films is determined by the energy of the walls as a function of position. Various effects originating in deviations from the ideal crystalline structure interact in a complex manner and determine the shape of a more or less statistical, irregular potential energy surface (PES). The dominating contributions to the PES arise from exchange and anisotropy inhomogeneities,[3,4] which are, on the other hand, directly related to the film structure and morphology. The PES thus provides a central link between film structure and magnetism. Important magnetic properties, such as coercivity and Barkhausen volume, follow directly from the distribution of energy barriers in the PES.

Overcoming these energy barriers requires activation energy, E_A. The application of a magnetic field or the increase of temperature decreases the effective barrier height. Experiments on the magnetization reversal process as a function of field *and* temperature therefore yield valuable information about the PES. Measurements of the magnetic aftereffect, commonly dubbed as magnetic viscosity, have turned out to be very helpful for the investigation of single activation events. Such experiments have been performed on thin films with perpendicular[5–11] and in-plane magnetization.[4,11] The interpretation of the results could be improved substantially by combination with magnetic imaging techniques, such as Kerr microscopy[7,9–11] or spin-sensitive scanning electron microscopy (SEMPA).[4] Thus, domain nucleation and wall propagation dominated magnetization reversal could be distinguished,[7,8,11,12] as predicted by Fatuzzis theory.[13] In some cases the experiments allow to estimate the Barkhausen volume, V_B,[5,8–10] or E_A.[4–6,10] The importance of domain pinning mechanisms,[11] roughness,[5,14] or preparation conditions[9] has been pointed out. The theoretical description of the observed data could significantly be improved by assuming distributions of E_A or V_B rather than constant values.[5,8] Temperature-dependent measurements of the magnetic aftereffect and the anisotropy would further allow us to improve the understanding of the correlation between film morphology and magnetism and provide a better understanding of the determining parameters for the Barkhausen volume, and thus for the PES. However, such experiments are extremely rare.

In this work, the magnetism and morphology of Fe films grown at low temperature on Cu(001) have been investigated as a function of temperature. Changes in the film morphology due to thermal activation and the consequences for magnetism can therefore be studied on one and the same film, allowing for a direct correlation between morphology and magnetic properties. The main achievement of this work is the determination of the distribution of energy barriers that control the coercivity, the Barkhausen volume, and the domain wall propagation.

II. EXPERIMENTAL

The experiments have been carried out in an ultrahigh vacuum (UHV) system consisting of a preparation and a magnetism chamber.[15] The preparation chamber is equipped with standard tools for substrate preparation, film deposition, and structural characterization. The sample temperature can be varied between 120 and 1300 K during preparation as well as characterization. The Cu substrates have been prepared by repeated sputter/annealing cycles.[16,17] The kinetic energy of the Ar^+ ions for sputtering is 500 eV. Sputter damages on the surface are removed by heating the sample up to 840 K between the sputter cycles. During the last annealing the sample is heated only to 650 K. From this temperature the sample is cooled down to RT slowly with a rate of

~0.5 K/s. This procedure has been found to be the best way to maximize the terrace width.

Fe is evaporated from a rod with a purity of 99.99% by electron bombardment heating. The Fe ion flux is kept constant during deposition by adjusting the electron acceleration voltage. The evaporation rate of the source is typically 0.8 Å/min and calibrated by depositing on a microbalance just before and after every film preparation. Furthermore, the deposition rate is checked with STM. Thus, an accuracy of the film thickness better than 0.1 atomic layers is achieved. Magnetic investigations have been performed on films of constant thickness, t_F, as well as wedge-shaped films with the thickness varying from 0 up to 12 ML. The height and length of the wedges are determined by the evaporation rate and the speed by which the sample is moved with respect to a metal shutter placed between the sample and the Fe source.

For magnetic characterization, the sample is transferred *in situ* into the magnetism chamber. Here, an electromagnet with yoke as well as a pair of Helmholtz coils produce external magnetic fields of up to 0.15 T within the film plane and 50 mT perpendicular to the film plane. The magnetic properties presented in this work are investigated by integral and laterally resolved magneto-optical Kerr effect measurements (MOKE). The former is used to obtain magnetization loops of a sample area of 50 μm^2. Longitudinal and polar geometry is used for studying the magnetization within the film plane and perpendicular to the film surface. The Kerr microscope is based on a commercially available Jenapol polarization microscope. It allows direct imaging the magnetization state of the sample over an area of 400 μm $\times$300 μm. For domain imaging the sample is placed directly in front of a strain-free quartz glass window with a flat bottom. Due to the shape of the window, a distance between sample surface and objective as small as 8 mm is possible. A lateral resolution of 0.5 μm and optical magnification of 10 can be achieved. Images are read out by a computer-controlled CCD camera with an acquisition rate of 4 s/image. The advantage of the setup is that changes in the magnetization state can be observed *in situ* and directly during thermal treatment.

III. TEMPERATURE DEPENDENCE OF THE MAGNETIZATION AND THE REVERSAL PROCESS

The magnetic properties of epitaxial Fe films grown at 120 K on Cu(001) are in the focus of extensive research due to the appearance of interesting structural and magnetic phases in the limit of ultrathin films.[16,18–22] Below the critical film thickness of t_{crit}=4.3 ML a spin reorientation transition (SRT) from in-plane to out-of-plane is observed. The presence of a perpendicular easy axis of magnetization is ascribed to the dominating surface anisotropy contribution arising at the film-vacuum interface, K_{f-vac}.[22]

It has been shown previously that t_{crit} depends sensitively on the electronic interaction with adsorbates[22] and on the sample temperature.[23] As an extension of the published work, in this paper we will focus on thermally induced structural changes and the consequences for the magnetism. Important information about the potential energy surface and its relevance for the magnetic properties of the sample are deduced.

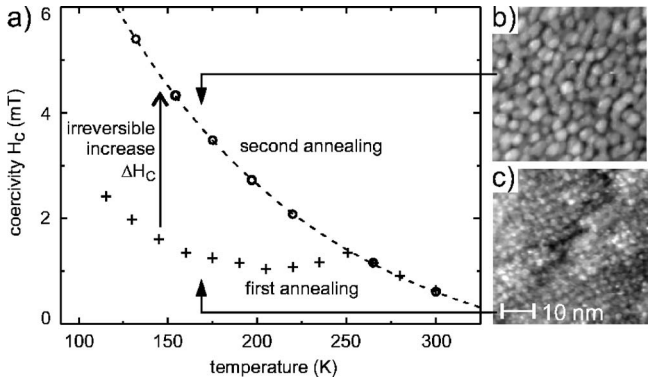

FIG. 1. (a) Temperature dependence of the coercivity of 3 ML Fe/Cu(001) during the first and second annealing cycles after growth at 127 K. The Fe island size at 296 K (b) is significantly increased compared to 165 K (c).

A. Correlation between film morphology and magnetic properties

The microstructure of epitaxial films determines the energy of a domain wall, $E(x)$, at the position x. Local variations of the energy provide obstacles for the wall propagation and determine the coercive field, H_C, of a sample. More precisely, H_C is related to the maxima of the gradient of the PES, $(dE/dx)_{max}$, averaged over the entire sample,

$$H_C \sim \sqrt{\left(\frac{dE}{dx}\right)^2_{max}}. \quad (1)$$

The coercivity of a thin magnetic film is thus directly correlated with its potential energy surface, which in turn is dependent on the film morphology.

The temperature dependence of H_C of 3 ML Fe grown on Cu(001) at 120 K is shown in Fig. 1(a). The data (+) measured on the as-grown film during the first annealing to 300 K after growth are markedly different from the reversible temperature dependence (○) of H_C found for all subsequent annealing cycles. Clearly, annealing of the as-grown sample up to 250 K irreversibly increases H_C. After reaching this temperature, the coercivity follows reversibly the temperature dependence given by the dashed line.

The morphology of epitaxial Fe on Cu(001) has been investigated as a function of temperature after the growth at 120 K by variable temperature scanning tunneling microscopy (VT-STM). The STM images in Figs. 1(b) and 1(c) reveal changes in the morphology of 3 ML Fe grown at 120 K upon annealing. Clearly, the average island size of roughly 5 nm at 296 K (b) is significantly increased compared to the island size at 165 K in Fig. 1(c), which is less than 1 nm. A more detailed analysis of the images shows that the rms roughness of the films changes only little during annealing, in contrast to the island width.

The increase of the island diameter with temperature is irreversible and occurs only during the first annealing after

the film growth. The islands reach the final size at 240 K. No further increase of the island size is observed for annealing up to 300 K.[23] It is therefore reasonable to attribute the irreversible increase of H_C to the thermally activated changes of the film morphology, i.e., the increase of the island size.

The islands introduce energy barriers for domain wall propagation due to exchange and anisotropy inhomogeneities.[3] The film morphology in Fig. 1(b) can be used to estimate the wall exchange energy variation, $\Delta\gamma$, at the island sites. The variation of the film thickness, $\Delta t_F = 4.8$ Å, results in $\Delta\gamma = 1\times10^{-11}$ J/m. Besides this exchange effect, also the magnetic anisotropy energy and the strain varies with island size, further contributing to the energy barriers at the island sites.

The Bloch domain wall width can be estimated using the expression, $\delta = \sqrt{At_F/K_S}$. By inserting the film thickness, $t_F = 5.4$ Å(=3 ML), $A = 2\times10^{-11}$ J/m, and $K_S = 1.49$ mJ/m^2 the wall width of $\delta = 6$ nm is obtained. The use of the bulk exchange stiffness A is a good approximation for films thicker than 1 ML; calculations for a bcc Fe(110) layer indicate that A is somewhat increased only at the surface of thin films,[24] in contrast to pure 2D systems.[25] It now becomes clear that the increase of H_C is related to morphological changes during annealing. In the as-grown film the islands are considerably smaller than δ. The wall therefore stretches over several islands and domain wall propagation is comparably easy. As the island width increases with temperature, eventually at 240 K the islands become comparable in size to the Bloch wall width, $L \approx \delta$. In this situation, the wall is being trapped between adjacent energy barriers. Higher external magnetic fields are necessary for wall displacement. Repeating the annealing cycle does not further change the island size, which explains that irreversible changes of H_C are only observed during the first annealing. The dependence of $H_C(T_a)$ (dashed line, $\sim T^{-1}$) is characteristic for a thermally activated overcoming of the energy barriers.

B. Magnetic aftereffect

The results discussed in the previous section show clearly that the coercivity is determined by the distribution of energy barriers that mainly originate from the Fe islands. Detailed information about the potential energy surface in Fe/Cu(001) can be obtained by measuring the time dependence of the magnetization, $M(t)$, for fields $H < H_C$ as a function of temperature.

MOKE hysteresis loops are recorded prior to the aftereffect measurement in order to determine H_C. A characteristic MOKE loop for 3 ML Fe/Cu(001) at 120 K is shown in Fig. 2. Typically, at H_C a magnetization somewhat smaller than the saturation magnetization, M_S, is achieved. A saturation field of $H_{sat} \sim 2H_C$ is required to achieve the fully saturated magnetization state, as reflected by characteristic tails in the hysteresis loop. The Kerr image in Fig. 2 reveals that domains of magnetization opposite to the field direction still exist at H_C. It will be shown in the following section that these domains, which are pinned to defects of the sample surface, are the result of the formation of energy-costly 360 deg domain walls.

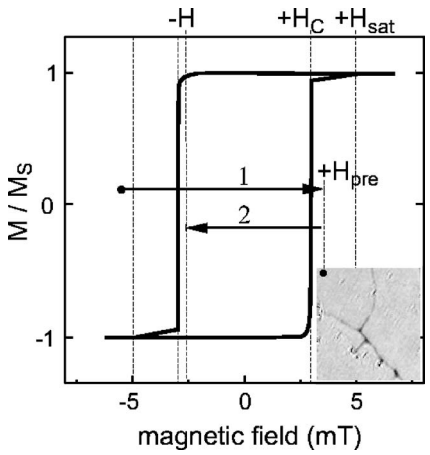

FIG. 2. MOKE magnetization loop of 3 ML Fe/Cu(001) at 120 K. The fields relevant for the after-effect measurements are indicated. Inset: Kerr image taken at H_{pre} showing nucleated domains. (Image size 70×70 μm^2.)

Prior to the measurement of $M(t)$ the sample is brought into a well-defined initial magnetization state $+\mathbf{M}$ with domains of opposite magnetization $-\mathbf{M}$ already nucleated (analog to the domain state shown in the inset in Fig. 2). This is achieved by sweeping the external field from $-H_{sat}$ to the premagnetization field $+H_{pre}$, where $+H_C < H_{pre} < +H_{sat}$ (step 1 in Fig. 2). At $t=0$, a negative field, $-H_C < H < 0$ (step 2 in Fig. 2), is turned on and kept constant for the duration of the experiment. The evolution of the sample magnetization with time, $M(t)$, is recorded with MOKE. At the end of the experiment the field is increased above $-H_{sat}$ to achieve the saturated magnetization state as a reference.

The time-dependent MOKE signal measured on 3 ML Fe at 120 K is shown in Fig. 3(a). At $t=0$, an external field of $H = -3.2$ mT $= 0.74\times H_C$ was applied. The magnetization reverses from $+M_\infty$ to $-M_\infty$ as a function of time due to thermally activated domain wall propagation. As was shown in previous work,[6] the time dependence $M(t)$ can be described by the following expression:

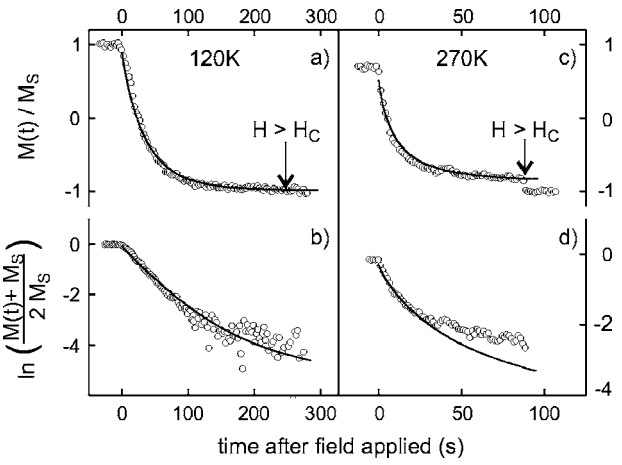

FIG. 3. Magnetic aftereffect of 3 ML Fe/Cu(001). (a), (b) $T = 120$ K, $H = -0.74\times H_C$; (c),(d) $T = 270$ K, $H = -0.77\times H_C$.

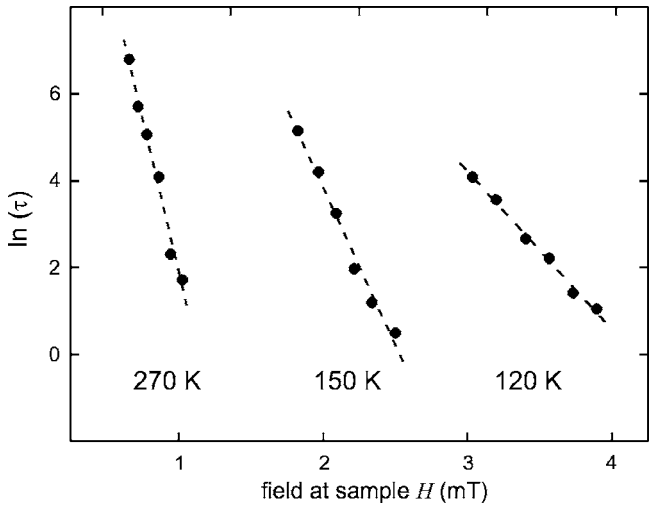

FIG. 4. Relaxation times as a function of temperature and external field, for 3 ML Fe/Cu(001) grown at 127 K.

$$M(t) + M_\infty = 2M_\infty \exp\left(-\frac{t}{\tau}\right). \tag{2}$$

M_∞ refers to the equilibrium or anhysteretic magnetization, and of course depends to some extent on H_{pre}. The exact value for M_∞ is not known, but a reasonable approximation is given by $M_\infty = M_S$. The time constant τ should follow an Arrhenius law,

$$\tau = \tau_0 \exp\left(\frac{E_A}{k_B T}\right), \tag{3}$$

and can be obtained from fitting $M(t)$. Experiments as in Fig. 3 were performed as a function of H, and the τ was determined for each experiment. The obtained data for $\ln \tau(H)$, measured at 120 K, are plotted as a function of the field in Fig. 4 for selected temperatures. The data show linear dependence on H. The slope of the data in this representation is directly related to the activation energy, E_A,

$$\ln \tau = \ln \tau_0 + \frac{E_A}{k_B T}, \tag{4}$$

which has to be a function of the field if $\ln \tau_0$ is assumed to be field independent,

$$E_A = M_S V_B (H + H_P). \tag{5}$$

This expression is valid for $-H_P \leqslant H \leqslant 0$. Here, the propagation field H_P is introduced. It corresponds to the field needed to reverse M without any activation process, and reflects the local slope of the PES, as was thoroughly discussed in Ref. 6. Temperature-dependent measurements of $M(t)$ should, in principle, yield H_P, as will be discussed later in this paper.

The slope m of the fit to the data in Fig. 4 corresponds to

$$m = \frac{M_S V_B}{k_B T}, \tag{6}$$

according to Eqs. (4) and (5). It directly yields the Barkhausen volume, V_B. For two-dimensional systems, such as the monolayer thin films presented here, it is more appropriate to use the expression Barkhausen *length*, l_B, rather than *volume*. The film thickness, t_F, is required for conversion,

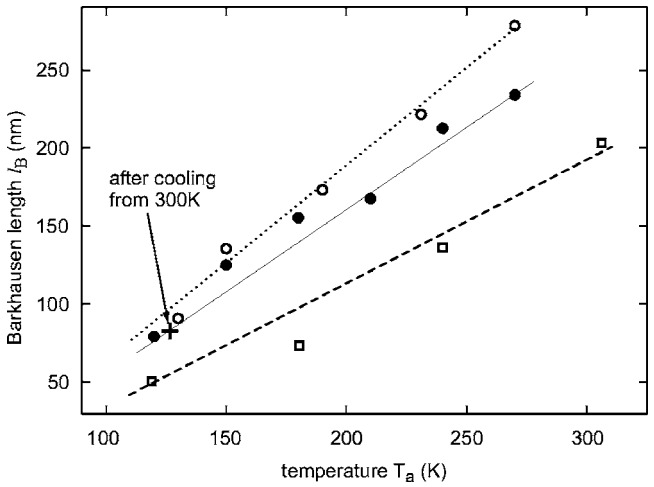

FIG. 5. Temperature dependence of the Barkhausen length, l_B, for Fe/Cu(001): 2 ML Fe grown at 127 K (□), 3 ML Fe grown at 127 K (●), 3 ML Fe grown at 300 K (○).

$$l_B = \sqrt{\frac{V_B}{t_F}}. \tag{7}$$

Following this recipe, a Barkhausen length of $l_B = 80$ nm is determined for the 3 ML Fe film on Cu(001) at 120 K.

Temperature-dependent measurements of the magnetic aftereffect are performed between 127 K and 300 K to obtain l_B as a function of temperature. Since the coercivity changes with temperature (see Fig. 1), smaller external fields are necessary to reverse the magnetization of the sample with increasing T. The $M(t)$ recorded at 270 K is shown in Fig. 3(c). Here, at $t=0$ the field $H = -0.95$ mT $= 0.77 \times H_C$ was applied. In analogy to the measurement at 120 K the magnetization reverses as a function of time. The main difference of this experiment compared to the measurement at 120 K is that $M(t=\infty)$ remains significantly smaller than M_S at the end of the experiment.

The l_B as a function of T is shown in Fig. 5 for 3 ML Fe grown at 127 K (●), 3 ML Fe grown at 300 K (○), and 2 ML Fe grown at 127 K (□). The data show that (i) the Barkhausen length is clearly a function of temperature. We find for 3 ML Fe grown at 127 K an increase by a factor of 3, from $l_B = 80$ nm at 120 K up to 240 nm at 296 K. The temperature dependence is fully reversible; after cooling the sample from $T_A = 300$ K down to 127 K, the $l_B = 80$ nm is again found (+). (ii) As a tendency, l_B increases with film thickness. (iii) The preparation condition influences the l_B only little. The atomically flat, high-quality Fe films prepared at 300 K show a l_B only slightly larger than that of the rough Fe films grown at low temperature. On the first glance, these results seem to suggest that the Barkhausen length is not determined by the morphology of the film. On a closer look, rather avalanchelike switching over multiples of the Barkhausen length occurs after a single activation event,

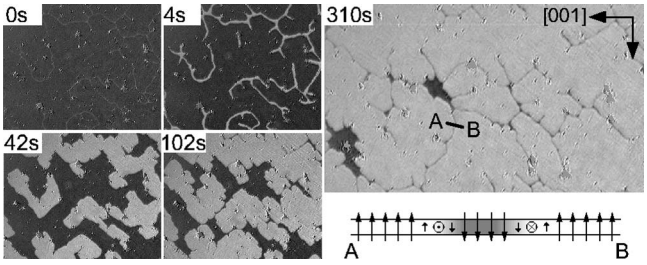

FIG. 6. Evolution of the magnetization of 3 ML Fe/Cu(001) after a magnetic field of $H=-0.97$ mT was applied at $t=0$ s. After 310 s narrow lines of original magnetization remain due to the formation of 360 deg walls preventing the fully saturated opposite magnetization state. Image size: 400×300 μm^2.

making the actually measured l_B insensitive to barriers on the atomic scale. This process will be discussed in the following section in more detail.

C. The magnetization reversal process

Details about the magnetization reversal process are revealed by *in situ* Kerr microscopy. The sequence of Kerr images in Fig. 6 shows the propagation of magnetic domains in 3 ML Fe during a viscosity measurement at 131 K. The dark/bright contrast in the images corresponds to magnetic domains in the film with opposite magnetization along the film normal. The elapsed time after the external magnetic field was applied is indicated within the images. Already nucleated domains barely visible at $t=0$ s start to grow with time, until the magnetization is almost completely reversed. As adjacent Bloch walls approach each other they are unable to merge for a single domain state. This slows down and finally stops the reversal process. Small lines of initial magnetization of width $d\approx5$ μm remain. These nonreversed areas are the result of the formation of 360° walls out of two adjacent 180° Bloch walls, as discussed by Bauer *et al.* for the case of Ni/Cu(001).[10] The removal of these walls is energy costly. A field almost twice the coercivity is required to form a fully saturated single domain state, as concluded from the magnetization loop in Fig. 2.

The Kerr images clearly show that the magnetization reversal is a propagation-dominated process. The activation energy for domain nucleation is significantly larger than the activation energy for wall propagation.

For a more compact and informative presentation of the time evolution of the domain state, the sequence in Fig. 6 is reproduced in the color-coded chart in Fig. 7(a). The colors represent areas subsequently occupied by the domains of magnetization parallel to H at the indicated time interval. For a comparison, the magnetization reversal at 131 K (a) and 291 K (b) are shown. At low temperature the domain walls propagate continuously in all directions. The propagation velocity is determined by the in-plane anisotropy of the Fe, thus the domain shape reflects a four-fold symmetry after some time. The nucleation sites for the domains are determined by macropins on the surface.

The domain propagation changes completely at an elevated temperature [Fig. 7(b)]. Here, the four-fold in-plane

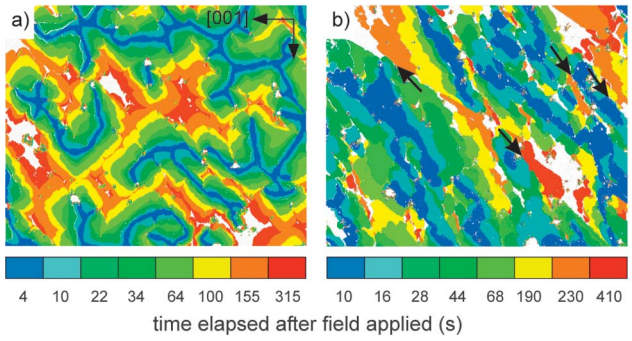

FIG. 7. (Color) A comparison of the domain wall propagation in 3 ML Fe/Cu(001) within a constant field at 131 K (a) and 291 K (b). The evolution of the domain size with time is color coded. Image size: 400×300 μm^2.

anisotropy does not show up in the domain shape. More strikingly, the wall propagation is discontinuous. On many positions, such as those marked by arrows, the domain propagation comes to a halt and proceeds intermittently. The transition from continuous to discontinuous wall propagation indicates a change in the activation process due to competing pinning mechanisms predominant at different temperatures. As will be discussed in the following chapter, a simple theoretical description of the viscosity experiments is only possible for the continuous wall propagation at low temperatures.

IV. DISCUSSION

The calculation of the activation energy, E_A, requires the intrinsic propagation field H_P [Eq. (5)], which can be deduced from the field- and temperature-dependent measurement of the relaxation times, τ, in Fig 4. The intercept y_0 of each fit with the y axis at $H=0$ is, according to Eqs. (4) and (5),

$$y_0 = \ln(\tau_0) + \frac{M_S V_B H_P}{k_B T}. \tag{8}$$

From the temperature dependence of y_0, a system of equations is obtained with H_P as one solution. For Fe/Cu(001) in Fig. 4, the y_0 turns out to be constant for all measurements, and thus independent of T. The slope, m, on the other hand, is clearly a function of T. A solution for H_P other than $H_P=0$ can therefore not be found. We conclude that the intrinsic propagation field itself changes with temperature. This proposed dependence, $H_P(T)$, is independent of the film structure since identical values for m and y_0 are found after repeated annealing cycles for one and the same film. Although the H_P cannot be calculated easily within this model, we can say that $H_P(T)$ has to depend inversely and reversibly on T.

To circumvent the difficulty of determining H_P we consider relaxation times, τ, rather than activation energies in the following. The relaxation times can be determined from the experiment directly and are equivalent to the activation energies, with the advantage that H_P and τ_0 are not required.

We use an approach introduced by Bruno *et al.* to obtain the distribution of τ as a function of H.[5] Starting from Eq.

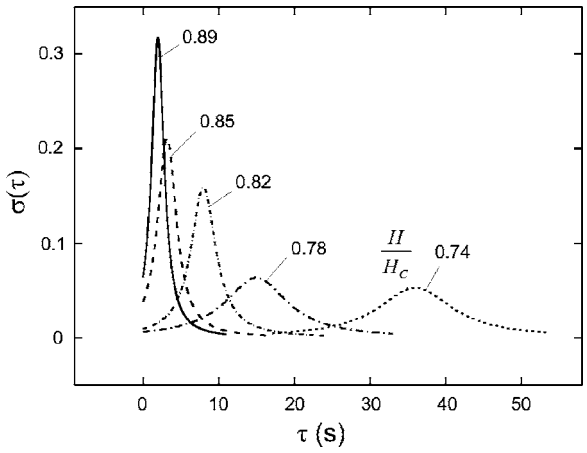

FIG. 8. Distribution of τ for 3 ML Fe/Cu(001) at 120 K for different H/H_C.

(2), the viscosity measurements in Figs. 3(a) and 3(c) are plotted as the logarithm of $[M(t)+M_S]/2M_S$. In such a presentation the data should depend linearly on t if there was no distribution of τ. As can be seen in Figs. 3(b) and 3(d), this is clearly not the case here. The data are therefore approximated by assuming a Lorentz distribution of τ,

$$\sigma(\tau) = \frac{\Gamma}{2\pi[(\tau-\tau^*)^2 + (\Gamma/2)^2]}. \tag{9}$$

The τ distribution of width Γ is centered around τ^*. At time t the total magnetization of the sample that is exposed to the field $H<H_C$ is the sum of the magnetization of all Barkhausen volumes with Lorentz-distributed τ,

$$M(t) = 2M_\infty \int_0^\infty \sigma(\tau)\exp\left(-\frac{t}{\tau}\right)d\tau - M_\infty. \tag{10}$$

The resulting fit to the viscosity measurement at 120 K, shown in Figs. 3(a) and 3(b) as a solid line, is in fairly good agreement with the data. The distribution $\sigma(\tau)$ determined from the data at 120 K as a function of field are shown in Fig. 8. The ratios H/H_C are indicated in the figure. One can see that the closer the applied field to H_C, the smaller the parameters τ^* and Γ of the fitted distribution, and thus the smaller and sharper the energy barriers.

The model yields a good description of the viscosity at 120 K, but it fails to describe the measurements at higher sample temperatures: Although a satisfying fit to $M(t)$ can be achieved [Fig. 3(b)], the same fit matches the data in the logarithmic presentation in (d) only in the early stage of the experiment. As time elapses the discrepancy between the data and the fit becomes significant.

The Kerr images in Fig. 7 visualize the difference between the magnetization reversal process at low and room temperature, and thus help to explain the failure of the model at higher temperatures. Clearly visible is the discontinuous domain propagation at 291 K versus the continuous wall propagation at 131 K. This qualitative change is interpreted as a change of the wall pinning mechanism with temperature. The sequence of Kerr images in Fig. 6 reveals that besides the micropins, which are intrinsic defects in the film correlated with its morphology, macropins also significantly influence the domain propagation. Such macropins are extrinsic defects spatially distributed on a 10–50 μm scale and directly recognizable in the Kerr images.[11] They visibly act as pinning centers for the domains. As can be seen, these macropins provide insurmountable obstacles in the temperature range up to 300 K. The formation of bcc crystallites within the fcc Fe film during cycling of the temperature between 120 K and 300 K, as found by Biedermann *et al.*,[26] might add additional pinning centers.

We conclude that the dominating wall pinning mechanism changes with temperature. As a result, a transition from continuous to discontinuous wall propagation at $\approx$250 K is observed, when micropins provided by the Fe islands become unimportant compared to the macropins. Such a change of the pinning is most likely the reason for the difficulty to determine the propagation field, H_P, as described at the beginning of this section. More important, it explains the failure to apply the viscosity model over the full temperature range. The theoretical description of the data does not consider competing activation mechanisms and therefore works best at low temperatures, where the micropins govern the magnetization reversal.

Due to the difficulties in determining the intrinsic propagation field, the activation energy cannot be calculated directly within this work. However, a rough estimate for H_P can be obtained by assuming $H_P=H_C(T=0)$. Extrapolation from Fig. 1 gives $H_P\approx 36$ mT, resulting in E_A to $\sim$1 eV. This value is comparable to the activation energy found for Ni/Cu(001) with $E_A\simeq 0.7$ eV,[10] or for Au/Co/Au films, where $E_A\sim 0.9$ eV.[5] It is interesting to note that the activation energy is thus orders of magnitude larger than the thermal energy ($\sim$10 meV) and the field energy ($\sim$0.3 μeV). The observed relaxation times, on the other hand, suggest that the ratio between the activation energy and the barrier height must be smaller than 1:10. This discrepancy shows that the model for the calculation of E_A provides only an upper limit. The result underlines the importance of the attempt frequency of a spin to overcome energy barriers, besides the barrier height itself, for the magnetization reversal process.

The reversible increase of the measured Barkhausen length is a result of the reduced effective barrier height at elevated temperatures. A domain wall overcomes ballistically many barriers once it is in motion after an activation event. The length of such a jump, of course, depends on T. The measured l_B is therefore much larger than the intrinsic Barkhausen length determined by the morphology. If the wall jump during such an avalanche is large versus the intrinsic Barkhausen length, changes in the film morphology during annealing influence the measured l_B only little, if at all. In this picture, rather the dominating role of the islands as energy barriers is supported instead of the substrate steps, as suggested previously.[9] Due to their comparatively large spacing, macropins are of no significance for l_B at any temperature.

V. CONCLUSION

The experiments on ultrathin epitaxial Fe films grown on Cu(001) at 120 K show unambiguously that annealing causes

reversible and irreversible changes of the morphology and the magnetism of the films. The coercive field of the samples increases irreversibly upon annealing, while the increase of the Barkhausen volume is fully reversible. The coercivity is correlated with changes of the film morphology that provides barriers for domain wall propagation.

The experiments show clearly that both the height *and* the distribution of the energy barriers within the films are decisive for the film magnetism. With increasing temperature or applied magnetic field the effective barrier height for magnetization reversal, and thus the necessary activation energy, decreases. As a consequence, the Barkhausen length increases with temperature. In contrast, the irreversible increase of the coercivity is interpreted as an efficient domain wall trapping due to a morphology-related change in barrier distribution while the barrier height itself remains unchanged.

The Fe islands have been found to shape the potential energy surface, which governs the domain wall propagation during magnetization reversal. The potential energy surface is thus providing the link between structure and important magnetic properties.

*Electronic address: a.enders@fkf.mpg.de; URL: http://www.mpi-stuttgart.mpg.de/kern

[1] U. Gradmann, in *Handbook of Magnetic Materials*, edited by K. H. J. Buschow (Elsevier Science Publishers B. V., New York, 1993), Vol. 7.
[2] J. Shen and J. Kirschner, Surf. Sci. **500**, 300 (2002).
[3] D. Sander, R. Skomski, C. Schmidthals, A. Enders, and J. Kirschner, Phys. Rev. Lett. **77**, 2566 (1996).
[4] S. Boukari, R. Allenspach, and A. Bishof, Phys. Rev. B **63**, 180402(R) (2001).
[5] P. Bruno, G. Bayreuther, P. Beauvillain, C. Chappert, G. Lugert, D. Renard, J. Renard, and J. Seiden, J. Appl. Phys. **68**, R5759 (1990).
[6] G. Bayreuther, P. Bruno, G. Lugert, and C. Turtur, Phys. Rev. B **40**, 7399 (1989).
[7] J. Pommier, P. Meyer, G. Pénissard, J. Ferré, P. Bruno, and D. Renard, Phys. Rev. Lett. **65**, 2054 (1990).
[8] J. Giergiel, J. Ferré, and D. Renard, IEEE Trans. Magn. **29**, 2518 (1993).
[9] A. Kirilyuk, J. Giergiel, J. Shen, and J. Kirscher, J. Magn. Magn. Mater. **159**, L27 (1996).
[10] A. Bauer, E. Mentz, and G. Kaindl, J. Magn. Magn. Mater. **198-199**, 489 (1999).
[11] R. P. Cowburn, J. Ferré, S. J. Gray, and J. A. C. Bland, Phys. Rev. B **58**, 11507 (1998).
[12] M. Labrune, S. Andrieu, F. Rio, and P. Bernstein, J. Magn. Magn. Mater. **80**, 211 (1989).
[13] E. Fatuzzo, Phys. Rev. **127**, 1999 (1962).
[14] Y.-P. Zhao, R. Gamache, G.-C. Wang, T.-M. Lu, G. Palasantzas, and J. T. M. D. Hosson, J. Appl. Phys. **89**, 1325 (2001).
[15] D. Peterka, A. Enders, G. Haas, and K. Kern, Rev. Sci. Instrum. **74**, 2744 (2003).
[16] J. Thomassen, B. Feldmann, and M. Wuttig, Surf. Sci. **264**, 406 (1992).
[17] J. Giergiel, J. Kirschner, J. Landgraf, J. Shen, and J. Woltersdorf, Surf. Sci. **310**, 1 (1994).
[18] H. Zillgen, B. Feldmann, and M. Wuttig, Surf. Sci. **321**, 32 (1994).
[19] R. Allenspach and A. Bischof, Phys. Rev. Lett. **69**, 3385 (1992).
[20] J. Giergiel, J. Shen, J. Woltersdorf, A. Kirilyuk, and J. Kirschner, Phys. Rev. B **52**, 8528 (1995).
[21] E. Mentz, D. Weiss, J. Ortega, A. Bauer, and G. Kaindl, J. Appl. Phys. **82**, 482 (1997).
[22] D. Peterka, A. Enders, G. Haas, and K. Kern, Phys. Rev. B **66**, 104411 (2002).
[23] A. Enders, D. Peterka, D. Repetto, N. Lin, A. Dmitriev, and K. Kern, Phys. Rev. Lett. **90**, 217203 (2003).
[24] S. Moràn, C. Ederer, and M. FaehnlePhys. Rev. B **67**, 012407 (2003).
[25] M. Pajda, J. Kudrnovský, I. Turek, V. Drchal, and P. Bruno, Phys. Rev. Lett. **85**, 5424 (2000).
[26] A. Biedermann, R. Tscheliessnig, M. Schmid, and P. Varga, Phys. Rev. Lett. **87**, 086103 (2001).